Mechanism of Phase Transition in dl-Methionine

Determining Cooperative and Molecule-by-Molecule Transformations

Ghasemlou, S.; Cuppen, H.M.

DOI
10.1021/acsomega.3c04846

Publication date
2024

Document Version
Final published version

Published in
ACS Omega

License
CC BY-NC-ND

ACS OMEGA

Open Access

http://pubs.acs.org/journal/acsodf

Article

Mechanism of Phase Transition in DL-Methionine: Determining Cooperative and Molecule-by-Molecule Transformations

Saba Ghasemlou and Herma M. Cuppen*

Cite This: *ACS Omega* 2024, 9, 3229−3239

Read Online

ACCESS | Metrics & More | Article Recommendations | Supporting Information

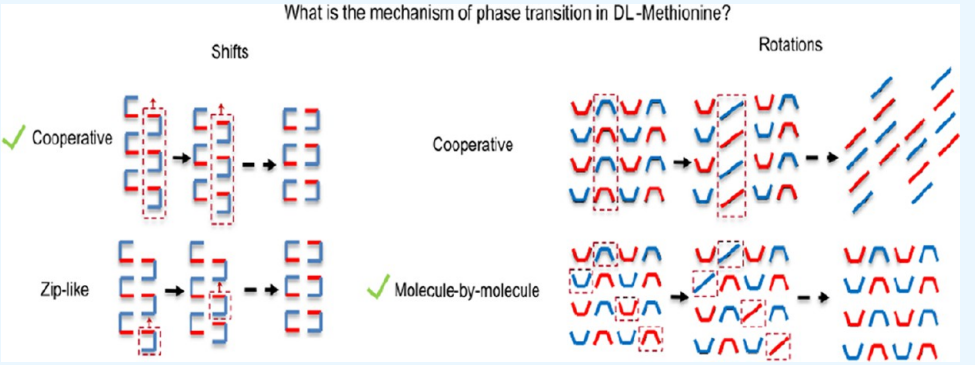

ABSTRACT: The solid-state phase transition in DL-methionine has been extensively studied because of its atypical behavior. The transition occurs through changes in the molecular conformation and 3D packing of the molecules. Phase transitions in racemic aliphatic amino acid crystals are known to show different behaviors depending on whether conformational changes or packing changes are involved, where the former is thought to proceed through a nucleation-and-growth mechanism in a standard molecule-by-molecule picture, and the latter through a cooperative mechanism. The phase transition of DL-methionine resembles the thermodynamic, kinetic, and structural features of both categories: a conformational change and relative shifts between layers in two directions. The present paper presents molecular dynamics simulations of the phase transition to examine the underlying mechanism from two perspectives: (i) analysis of the scaling behavior of the free energy barriers involved in the phase transition and (ii) a structural inspection of the phase transition. Both methods can help to distinguish between a concerted phase change and a molecule-by-molecule or zip-like mechanism. The free energy predominantly scales with the system size, which suggests a cooperative mechanism. The structural changes draw, however, a slightly more complex picture. The conformational changes appear to occur in a molecule-by-molecule fashion, where the rotational movement is triggered by movement in the same layer. Conformational changes occur on a time scale nearly twice as long as the shifts between layers. Shifts in one direction appear to be less concerted than shifts in the perpendicular direction. We relate this to the edge-free energy involved in these shifts. We believe that the behavior observed in DL-methionine is likely applicable to phase transitions in other layered systems that interact through aliphatic chains as well.

INTRODUCTION

Solid materials can often exist in more than one crystalline form, so-called polymorphs, and the phenomenon is referred to as polymorphism. Molecular compounds can have structural differences due to differences in the conformation of the individual molecules and/or the 3D arrangement of the molecules in the crystal. The former is called conformational polymorphism, and the latter is packing polymorphism.[1,2] Polymorphic forms of the same compound show different physicochemical properties, such as dissolution rate, crystal shape, or crystal color.[3] Because of this, some forms find application in industry, while other forms are undesired. A common issue is the polymorphic phase transitions of the product under unforeseen circumstances.[4−6] In the pharmaceutical industry, this changes the efficacy and the bioavailability of the drugs. Therefore, it is vital for industries, including dye, food, pigment, and explosives,[7−9] to produce the favored polymorphic form and guarantee its maintenance in the final product. This is achieved by gaining knowledge about the mechanism of the polymorphic phase transitions, including their thermodynamics and kinetics.

Received: July 6, 2023
Revised: August 30, 2023
Accepted: September 4, 2023
Published: January 8, 2024

In general, phase transitions are classified as first order and second order. In a first-order type, there is a discontinuity in the first derivatives of the free energy, and for a second-order type, the discontinuity is in the second derivatives.[10] In the context of solid-state chemistry, the polymorphic phase transitions are classified according to their underlying mechanism as nucleation-and-growth and cooperative. The nucleation-and-growth mechanism is a common first-order phase transition including a molecule-by-molecule transformation between the conformational polymorphs.[11,12] The existence of second-order phase transitions is refused by Mnyukh since he proved that many phase transitions that were claimed to be second order are first order if they are studied in higher resolution. According to Mnyukh, all phase transitions are first order and proceed in a molecule-by-molecule fashion with or without an orientational relationship between the parent and daughter phases.[12] Due to the limitations of Mnyukh's theory in explaining complex transitions, the second-order type has gradually been supplanted by the cooperative mechanism, which incorporates a finite transition length scale ranging up to hundreds of molecules. Nevertheless, in the chemical literature, the clear distinction between cooperative and molecule-by-molecule nucleation-and-growth transitions is not commonly observed.[6,13−43] In the cooperative mechanism, often the crystal packing changes without influencing the molecular conformation.[17,44] Compared to the second-order classification, the length scale is finite. In a computational study of the first-order transition of DL-norleucine and L-phenylalanine, we found the transition to occur through a cooperative mechanism.[45,46] We speculated that the initial nucleus, of finite length scale, is formed in a cooperative way after which the transition further propagates. Here, the packing defect density is important in determining the initial nucleus size. We refer to this initial nucleus as the *critical cooperative segment*, and its size is likely to coincide with a maximum in the free energy for nucleation. This is similar to the critical nucleus concept in standard nucleation theory, formed in a molecule-by-molecule fashion. We will return to the concept of the critical cooperative segment in the conclusion.

The fact that a phase transition is first order does not give information about the mechanism of the transition: molecule-by-molecule or cooperative. Smets et al.[47] classified the phase transitions in racemic aliphatic amino acids into three different categories: (I) involving pure shifts, (II) with changes in the terminal torsions (outer torsion), and (III) with changes in torsions other than the terminal one (inner torsion). The phase transition in each class has different characteristic kinetic and thermodynamic features, which are linked to differences in the mechanism.

The nucleation-and-growth theory applies more to the molecule-by-molecule type, and it does not address more complex behaviors such as a zip-like mechanism[48] or cooperative phase transitions via rotation, displacement, and/or order−disorder transitions.[49] For the molecule-by-molecule type, the rate of transition is very low, up to hours or days, since the phase boundary line propagates in a molecule-by-molecule manner. The parent and daughter phases have often different conformational arrangements, and the corresponding enthalpy and entropy of the transition are large but the amount of hysteresis is small. Within the cooperative category, usually, the crystal packing is altered by overcoming relatively weaker nonbonded energy barriers. The molecular conformation between daughter and parent structures is similar, and this preserves the crystal integrity. The kinetic barrier for the cooperative phase transitions is high, but once it is surmounted, the transition proceeds very fast. The variation of the enthalpy and entropy is small, and the amount of hysteresis is large.

The solid-state phase transitions that proceed with a cooperative mechanism are often more interesting since they occur in versatile forms in molecular crystals such as bending, wriggling, self-actuating, exploding, and changes in their physical appearance.[50−53] In some cases, these changes are accompanied by a sudden release of energy that leads to a crystal jump. The crystals showing this behavior are known as jumping crystals. They are very interesting materials to be used in medical devices, actuators, and electronic sensors[54−61] This paper presents a computational study of the $\alpha \leftrightarrow \beta$ phase transition in DL-methionine (DL-Met) with the aim to unravel the mechanism of the phase transition. DL-Met is a member of the class of linear-chain racemic amino acids. Polymorphic phase transitions have been extensively studied in linear-chain racemic amino acids.[18,24,47,62−66] This group of compounds shares similar crystal structures. The interaction between the zwitterionic amino and carboxylic acid groups forms hydrogen-bonded bilayers, and the bilayers stay connected via the vdW interaction between the aliphatic side chains. In most of these structures, the phase transition takes place via either rotation of the side chains or sliding of bilayers in the vdW connections. The hydrogen-bonding pattern, however, stays intact. Only in DL-methionine with a high density of defect sites[67] and in DL-cysteine do the hydrogen bonds break and reform during the phase transition.[68]

A hybrid computational-experimental study by Shi's group has unraveled the role of defect sites in the phase transition of DL-Met.[67] They show that the phase transition is a one-step process in a single crystal based on differential scanning calorimetry (DSC) measurements. The low activation energy of the phase transition and large kinetic hysteresis for crystals with a low defect density indicate that the underlying mechanism is cooperative. For samples with a high defect density, a second peak is observed in the DSC, consistent with a two-step process. The second step is sensitive to the defect density and is suggested to follow a nucleation-and-growth mechanism. MD simulations confirm this scenario on a molecular level: the phase transition goes via the cooperative shifting of bilayers in the absence of defects, while in the presence of many defect sites, the phase transition occurs in two steps. First, there is a cooperative shifting of bilayers at the defect-free sites, and second, the hydrogen bonds break and reform with a nucleation-and-growth mechanism.

Previously we carried out a molecular dynamics study on DL-Met focusing on the phase transition in a defect-free crystal.[69] We obtained energy landscapes, including free energy and potential energy contributions to the transition. The free energy is suggestive of two distinct transition pathways; in one pathway, the transition initiates via shifts along the b axis followed by shifts along the c axis and conformational changes. In the other pathway, the two latter changes occur first, and the shifting along b follows. The study further shows that the energy is a balance between van der Waals interactions which are stronger in the β form and dihedral bonding, which is more favorable in the α phase. In this study, we investigate the contribution of the shifts and rotations to the phase transition and their influence on the phase transition mechanism from two angles. One is the scaling behavior of the free energy with

https://doi.org/10.1021/acsomega.3c04846
ACS Omega 2024, 9, 3229−3239

respect to the system size, and the other is the variance corresponding to shifting of bilayers and rotation of the terminal torsions. This information together with the inspection of the structural changes has provided novel insights into the phase transition mechanism.

COMPUTATIONAL SETUP

A similar computational setup to ref 69 is used.

Molecular Dynamics Setup. The initial α structure is obtained from CSD entry DLMETA07 in a $P2_1/a$ setting (Table 1). The size of the simulation box is defined by the number of unit cells along a, b, and c vectors, respectively. This value along a also defines the number of hydrogen-bonded bilayers in the simulation cell and a minimum of two replicas are needed to form at least one *vdW* connection. Including more bilayers complicates the phase transition and cannot be modeled using the current CVs as discussed below. In directions b and c a minimum of four and two replications are required, respectively (see 2). This is because the cutoff distance, which is 10 Å, needs to be smaller than half of the shortest simulation box vector. MD simulations are performed by LAMMPS[70] package and the collective variable calculations and the additional bias are performed by PLUMED-2.3.1[71−73] interfaced with LAMMPS-7Aug2019. The simulation results are visualized by VMD-1.9.3 program.[74−81] The Antechamber package was used to generate the Amberff15ipq force field parameters and charges for refs 82−85. The long-range interactions are calculated using pppm method with a relative accuracy of 10^{-4}.[86] The Lennard-Jones interactions are calculated with a cutoff value of 10 Å. The time integration is performed using the Nose−Hoover method in the isothermal−isobaric (NPT) ensemble.[87] Thermostat and barostat parameters were set to 40 and 400 fs, respectively.

2D Umbrella Sampling. Using the 2D umbrella sampling method, we run a series of MD simulations with harmonic constraints acting on d_b and s. Each simulation job with a specific d_b and s combination is called a "window". Table S1 summarizes the harmonic force constants for each CV and each system. The same fixed path-CV is used for all simulation box sizes and was converged for a system of 2 × 8 × 4 as described in ref 69. Each window starts with 100 ps of equilibration, while inner torsions and z (indicating the distance of the sampled configurations from the initial path) are restrained. Then, the restraints are released, and only the harmonic constraints acting on d_b and s remain. The window sampling starts from d_b = 0 and s = −0.05 and we increment s by 0.1 until s = 1.05. Then, the s is further sampled in the reversed direction (s = 1.0−0.0 with increment −0.1). This procedure is repeated for d_b = 0.1 until d_b = 1.0 is reached. Once the simulations are complete the output is processed via the weighted histogram analysis method (WHAM)[88] to estimate the free energy.

Table 1. Lattice Parameters of α and β Forms[a]

polymorph	α-form[90,90]	β-form[65]	β-form[89]
temperature (K)	340	320	320
space group	$P2_1/c$	$C2/c$	I2/a
a (Å)	16.811	31.774	33.0764
b (Å)	4.7281	4.6969	4.6969
c (Å)	9.886	9.8939	9.8939
β (°)	101.951	91.224	106.177
Z/Z'	4/1	8/1	8/1

[a]The parameters in $P2_1/c$ and $C2/c$ settings are reproduced here with permission of the International Union of Crystallography:[89] DOI1, DOI2.

STRUCTURE OF α AND β-DL-METHIONINE AND COLLECTIVE VARIABLES

The present paper focuses on the $\beta \rightarrow \alpha$ phase transition in DL-Met.[89] This transition is found to occur upon heating with a transition temperature between 306 and 307 K and a hysteresis of 20 K. Table 1 gives the crystallographic unit cell information on both forms. The cell axes in crystal structures can be chosen in different ways, depending on the position of the various symmetry operations. Using the standard conventions for space groups 14 ($P2_1/c$) and 15 ($C2/c$), the a axes in both structures do not align. Conversion from $C2/c$ to I2/a settings leads to a cell choice for the β polymorph that is more directly comparable to that of the α settings. Figure 1 compares the two polymorphic forms in the latter setting and along different projections. The molecules in the center are colored to indicate their chirality pattern, with the D-enantiomers colored pink and the L-enantiomers in blue.

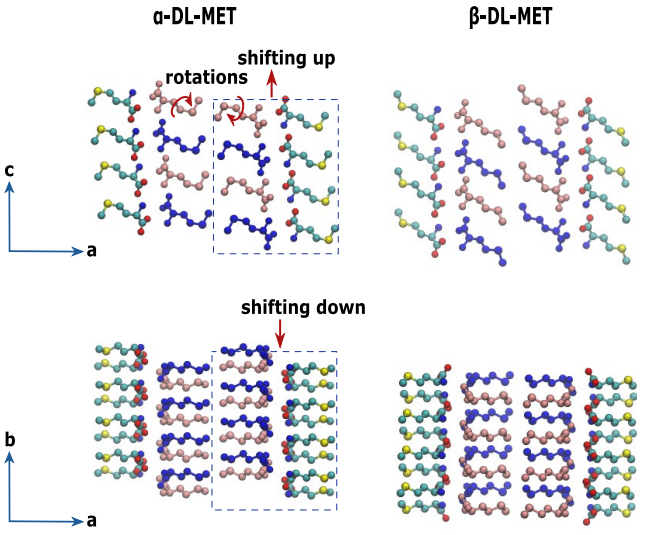

Figure 1. Phase transition in DL-Met. Pink and blue colors represent the D- and L-enantiomers, respectively. The changes are displayed in the $a-b$ and $a-c$ projections.

The phase transition occurs through shifts in the planes of the bilayers. These shifts occur parallel to the b and c lattice vectors, between the bilayers with the hydrophobic interactions. The shifts are clearly visible when the chirality pattern is compared between the layers. In the phase transition from α to β, a D-L pattern in the (a, b) plane changes to a D-D and L-L pattern. The reverse occurs in the (a, c) plane, where the D-D and L-L patterns change to D-L and L-D. The conformational transformations occur via the rotation of the C−C−S-C torsions. This dihedral change is most visible in the (a, c) projection.

In the simulations, the transition will be enforced by applying bias potentials to help the system cross the barrier for transition on a time scale that is still tangible for molecular dynamics simulations. This type of enhanced sampling molecular dynamics simulation requires that the phase transition be described by so-called collective variables

https://doi.org/10.1021/acsomega.3c04846
ACS Omega 2024, 9, 3229−3239

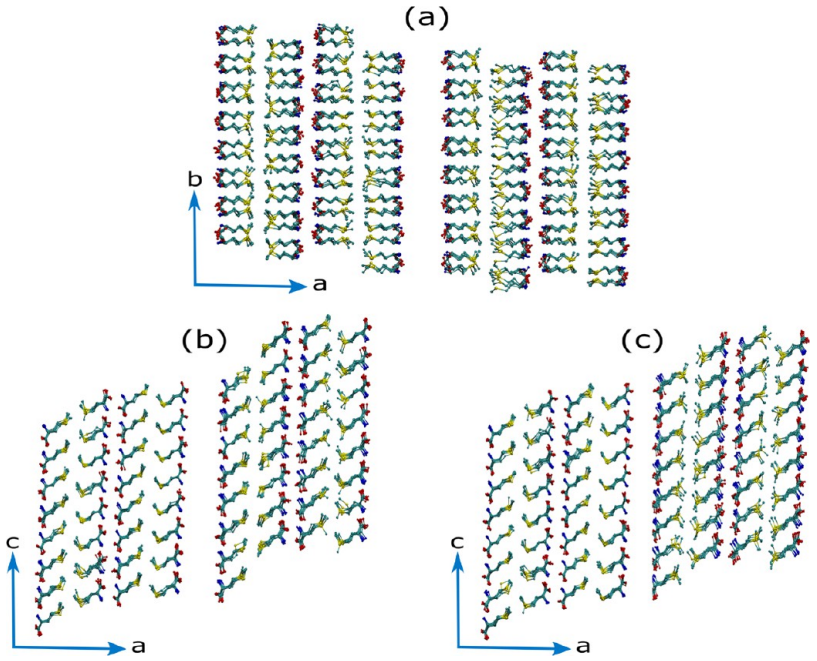

Figure 2. Snapshots with a high and low variance in a) d_b, b) d_c, and c) t. The left side of each panel is the low-variance state, and the right side is the high-variance state.

(CVs). These CVs indicate the similarity of a given structure, defined by its (x,y,z)-coordinates and the size and shape of the simulation box, to the two reference structures, in this case, the α and β polymorphic forms. Ideally, CVs reflect the reaction coordinates for the phase transition.

The same set of collective variables (CVs) was used as introduced in ref 69. In this work, the simulation cells have two replications in the a direction, which gives two bilayers. A total of six CVs were used: d_{b1} and d_{b2} which describe the shifts of the two bilayers along the b axis, d_{c1} and d_{c2} which describe the shifts of the two bilayers along the c axis, and t_α and t_β, which describe the fraction of molecules in the α or β torsional configuration, respectively. The four distance parameters were obtained by using the distance between two S atoms belonging to two methionine molecules of the same handiness in opposing bilayers. The d_b and d_c CVs use the distances projected along the b and c axis, respectively. The d_{b1} and d_{b2} CVs mostly affect the (a, b) plane, whereas the d_{c1}, d_{c2}, t_α, and t_β predominantly affect the (a, c). We have hence combined the two groups of CVs into a distance variable d_b and a path collective variable s containing d_{c1}, d_{c2}, t_α, and t_β. s shows the progress with respect to the path and changes within 0 and 1 or from a fully ordered α state and to an ordered β state. For a more in-depth discussion, we refer to Ghasemlou et al.[69]

All distance CVs, d_{b1}, d_{b2}, d_{c1}, and d_{c2}, are in fractional coordinates relative to the crystallographic unit cells. Increasing the simulation cell in the b and c direction will therefore not affect their value for the stable α and β forms. Similarly, the stable t_α and t_β values remain unaffected upon changes in the simulation cell size. We hence expect the free energy minima corresponding to the α and β phases to occur at the same CV values irrespective of the simulation cell size. If the simulation cell is expanded in the a direction, the number of bilayers changes, and therefore the number of CVs describing the shifts along the b and c axis also changes. In that case, it is not straightforward how to combine the CVs in a way that each visited configuration in $a \leftrightarrow b$ is described with a unique value. We hence limit our study to the layer size dependence of the transition, and we do not include the dependence on the number of bilayers. A proof of concept on the adequacy of the employed cell size is that with a simulation cell containing 2 × 8 × 4, we could capture the critical cooperative segment and estimate the energy barrier as explained in our previous study.[69] Our calculations returned a transition energy barrier of Eb/R = 1500 K per unit cell, which is almost twice the value obtained experimentally (Eb/R = 44100 K).[67] The four distance CVs describe the average positioning of the bilayers with respect to each other. This is based on an average of many distances and does not contain any information about the cooperativity of the slide. A "zip-like" slide in which the molecules shift one by one gives the same change in the CV as a mechanism in which all molecules shift simultaneously. We have hence devised additional parameters σ^2_{b1}, σ^2_{b2}, σ^2_{c1}, and σ^2_{c2} that describe the variance in the individual distances between bilayers (d_{b1},d_{b2}, d_{c1}, and d_{c2} that make up the layer average position). If the variance is high, this corresponds to a zip-like mechanism, whereas a low σ^2 is an indication of a cooperative mechanism. Figure 2 shows two snapshots of a phase transition simulation. The distances with indices 1 and 2 correspond to the left and right interfaces, respectively. In Figure 2a (left), σ^2_{b1} has a rather low value of 0.0024 and σ^2_{b2} has a value of 0.0077. Indeed, we can see that all of the molecules nicely line up. The values for d_{b1} and d_{b2} are −0.47 and −0.91 in this case, and it can be seen that the left interface is close to the α position while the right interface is closer to the β position. Figure 2a (right) shows an example of high variance; σ^2_{b1} is 0.046 in this case. The atoms, especially the sulfur atoms, have dispersed along b for the left interface. The right interface has again a low variance of 0.0045. In the high-variance case of d_b, it is not so clear whether this is due to a high conformational disorder or if that is mostly due to the distribution of S−S distances along b. This is especially because the corresponding σ_t of each interface is high, about 0.3, while one interface shows a high variance in d_b and the

https://doi.org/10.1021/acsomega.3c04846
ACS Omega 2024, 9, 3229−3239

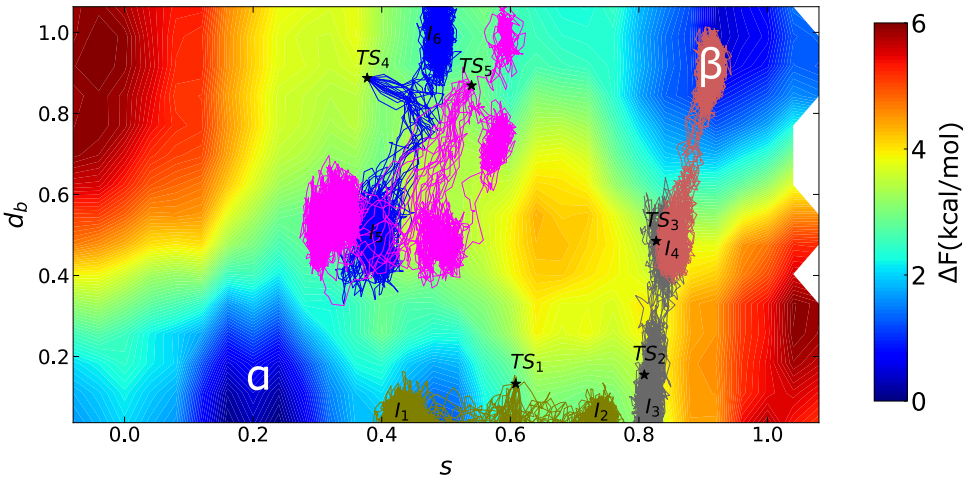

Figure 3. Free energy surface for the structure with 2 × 8 × 4 unit cells along *a*, *b*, and *c* vectors, respectively. The transition states (displayed with stars) and the two basins connecting to each transition state are labeled as TS_i and I_i/β, respectively. The unbiased trajectories initiated from each transition state are displayed in different colors.

other has a low value. The corresponding d_{b1} and d_{b2} are −0.68 and −0.45, respectively. The left interface is in between the stable states, and the right one is closer to the α position.

Figure 2b (left) is again a low-variance configuration; this time considering shifts along *c* with σ^2_{c1} = 0.0011 and σ^2_{c2} = 0.008, respectively. The corresponding distances are d^1_c = −0.11 and d^2_c = −0.32, respectively. In this state, both interfaces are highly lined up and have a position in between the stable states. Figure 2b (right) is a state with a high variance of σ^2_{c1} = 0.0037 and σ^2_{c2} = 0.0033 in both bilayers. d_{c1} = −0.45 and d_{c2} = 0.44; thus, both interfaces are close to the β position. This is while in the left interface, nearly all torsions are in the α form but in the right one, half of the torsions are in the α and the other half are in the β form.

For the torsional changes, it is less straightforward to come up with a measure for the cooperativity since here the number of molecules within a certain torsional range is used to follow the phase transition. It does not give information about the progress from one torsion to the other. This is partly because of the periodic nature of dihedral angles, which do not allow for a similar description to the distances. Instead, we devised a measure that can distinguish a layer-by-layer transition from a molecule-by-molecule transition that occurs homogeneously throughout the simulation box. First, three torsional CVs for each of the four layers are constructed: one giving the fraction of molecules within the α range, $t_{\alpha i}$, one within the β range, $t_{\beta i}$, and a combination of the two $t_i = t_{\alpha,i} - t_{\beta,i}$. A variance measure using the t_i's can be used to distinguish between the molecule-by-molecule and the layer-by-layer behaviors. The lowest variance is σ_t = 0.0012 with t_α = 0.31 and t_β = 0.31 and the highest variance is σ_t = 0.4 with t_α = 0.30 and t_β = 0.32. Figure 2c (left) shows a low variance, thus it is highly ordered, and the molecules align to a great extent. Both interfaces are in an intermediate position where in one layer the torsions are in the α form and in the other one in the β form. In Figure 2c (right), the variance is much higher since the torsions occupy a large range of forms from α to β. Although the t_α = 0.30 and t_β = 0.32 are very similar to the low variance form the distribution of the dihedral angles along the average value is not similar, leading to the structures with very different variances of rotations. The variance of changes for the rotations is much higher compared to the shifts. This should be because the rotations occur in a single-molecule to single-molecule manner while the shifting of bilayers is concerted.

RESULTS AND DISCUSSION

Figure 4 shows the Helmholtz free energy surface as a function of the collective variables for four different system sizes: (a) 2 × 4 × 2, (b) 2 × 8 × 2, (c) 2 × 4 × 4, and (d) 2 × 8 × 4 replications along *a*, *b*, and *c* lattice axes, respectively. The energies are scaled per unit cell, and the color gradient covers the same range in all panels. A first glance all panels show that they are indeed very similar: the stable states are in the same positions, and the dynamic range of the graphs covers more or less the same scale. This means that the barriers for the transition roughly scale with the system size, indicating a collective mechanism for the phase transition. All four free energy surfaces show roughly two routes to connect α and β: one where first *s* changes and then d_b and the other way around. Changing d_b and *s* simultaneously is hampered by a significant barrier around $(s,d_b)=(0.7,0.5)$, which is present for all sizes. We performed a committer analysis to find transition states in the free energy surface for the largest cell size of 2 × 8 × 4. The results are plotted in Figure 3. For this, unbiased MD simulations were performed at different starting locations to find the transition states from which roughly half of the trajectories evolved to α or an intermediate state toward α and the other half of the trajectories evolved to β or an intermediate state toward β. As the figure shows, several transition states need to be overcome to reach β starting from α or *vice versa*. In Figure 3, transition states are indicated by stars and have labels TS_i and intermediate states are displayed as I_i.

For the path connecting α to β through transition states 1−3, a nearly fully connected pathway is obtained; for the transition via TS_4 and TS_5, this was not possible. The unbiased simulations revealed that the free energy surface is rather flat but with many local free energy minima in the region around TS_4 and TS_5. Unbiased simulation leads to many different local minima starting from these points; several at very close distances in CV space. Thus, distinguishing between all minima and transition states connecting them is not feasible; and perhaps not so informative either. We will hence limit our discussion to the ones labeled in Figure 3. TS_1 connects two

https://doi.org/10.1021/acsomega.3c04846
ACS Omega 2024, 9, 3229−3239

Table 2. Free Energy Value Corresponding to Each Transition State (1−4) and in Structures with (a) 2 × 4 × 2, (b) 2 × 8 × 2, (c) 2 × 4 × 4, and (d) 2 × 8 × 4 Unit Cells ($Z = 4$)[a]

	ΔF (kcal/mol)							
simulation cell size	$I_1 \rightarrow TS_1 \rightarrow I_2$		$I_3 \rightarrow TS_2 \rightarrow I_4$		$I_4 \rightarrow TS_3 \rightarrow \beta$		$I_5 \rightarrow TS_4 \rightarrow I_6$	
(a) 2 × 4 × 2 = 16	0.37	−0.17	0.39	−0.24	0.01	−0.67	0.27	−0.77
(b) 2 × 8 × 2 = 32	0.49	−0.16	0.25	−0.09	0.09	−0.68	0.27	−0.74
(c) 2 × 4 × 4 = 32	0.36	−0.18	0.36	−0.17	0.05	−0.64	0.25	−0.84
(d) 2 × 8 × 4 = 64	0.38	−0.06	0.21	−0.15	0.08	−0.66	0.18	−0.70

[a]The energies are scaled per unit cell.

states, which differ in s, while for barrier TS_2, the difference is in d_b. For TS_3 and TS_4, both variables change.

MECHANISM OF THE TRANSITION

So far, we focused on the thermodynamic aspects of the transition and have not considered the mechanism of the transition. The scaling behavior of the barrier heights for the transition with the system size should give some indication. In the traditional picture of the nucleation-and-growth mechanism, a critical nucleus has to form, and the barrier is related to the free energy cost of the formation of the nucleus. The critical nucleus size is independent of the system size as long as it is smaller than the system size. The barrier height should hence be independent of the system size. In the case of a cooperative mechanism, the number of molecules that are involved in the transition scales linearly with the system size, and the barrier height is expected to scale accordingly.

We focus on barriers 1−4 that have been identified in the previous section. Table 2 indicates their heights relative to their two connecting intermediates for each of the free energy surfaces presented in Figure 4 and is given in units of kcal/

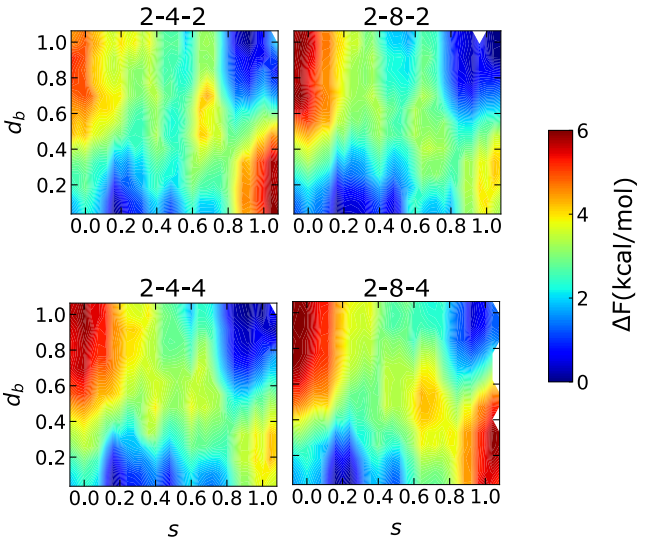

Figure 4. Free energy surfaces for structures with $n_a \times n_b \times n_c$ unit cells along a, b, and c lattice vectors, respectively.

(mole unit cell). Most free energy differences are very similar for all four cell dimensions. The only clear exception is for $I_3 \rightarrow TS_2$, which has a higher barrier for the cell sizes which have only 4 replications in the b direction. This transition mainly involves changes in d_b. The other barriers appear to scale linearly with system size, which hints at a cooperative mechanism. We had anticipated that changes in d_b and d_c would scale linearly, whereas changes in torsions lead to a different scaling behavior since they are less likely to rotate simultaneously and more in a molecule-by-molecule fashion, but this cannot be concluded from looking at the barrier heights alone.

The committer analysis simulations can be used to study the transition from a more structural perspective. The free energy surfaces were obtained from an umbrella sampling simulation, and their trajectories show a sampling of CV space and do not necessarily reflect the transition mechanism. Unfortunately, a spontaneous transition cannot be simulated as this would take too long to cover by MD simulations, but in the committer analysis, the system is allowed to spontaneously evolve starting from the energy barrier. We hope that the mechanism "downhill" reflects the mechanism "uphill" that we are not able to simulate.

Here we will discuss the transition in terms of $\alpha \rightarrow \beta$ to make it easier to follow, but the discussion should also hold for the reverse transition. Figure 5 depicts the structure of the transition states in different projections. In Figure 6, d_{bi} and d_{ci} represent the shifts parallel to the b and c lattice vectors,

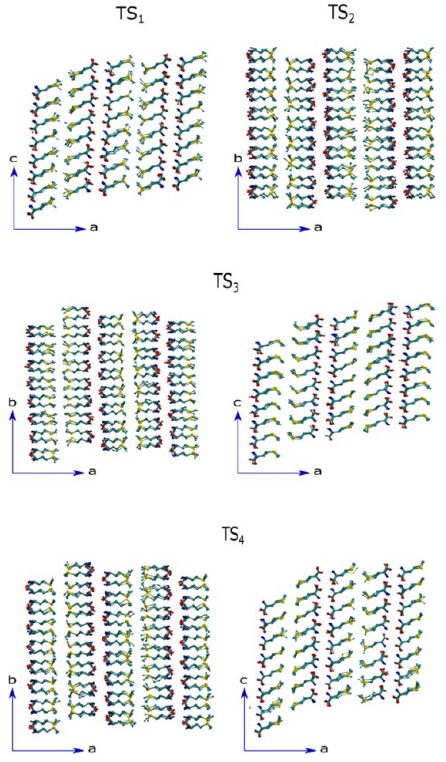

Figure 5. Structure of the transition states (TS_1 to TS_4) in (a, b) and (a, c) projections. TS_1 and TS_2 connect the states, which differ in a−c and a−b projections, respectively. For the rest, the differences are observed in both projections.

https://doi.org/10.1021/acsomega.3c04846
ACS Omega 2024, 9, 3229−3239

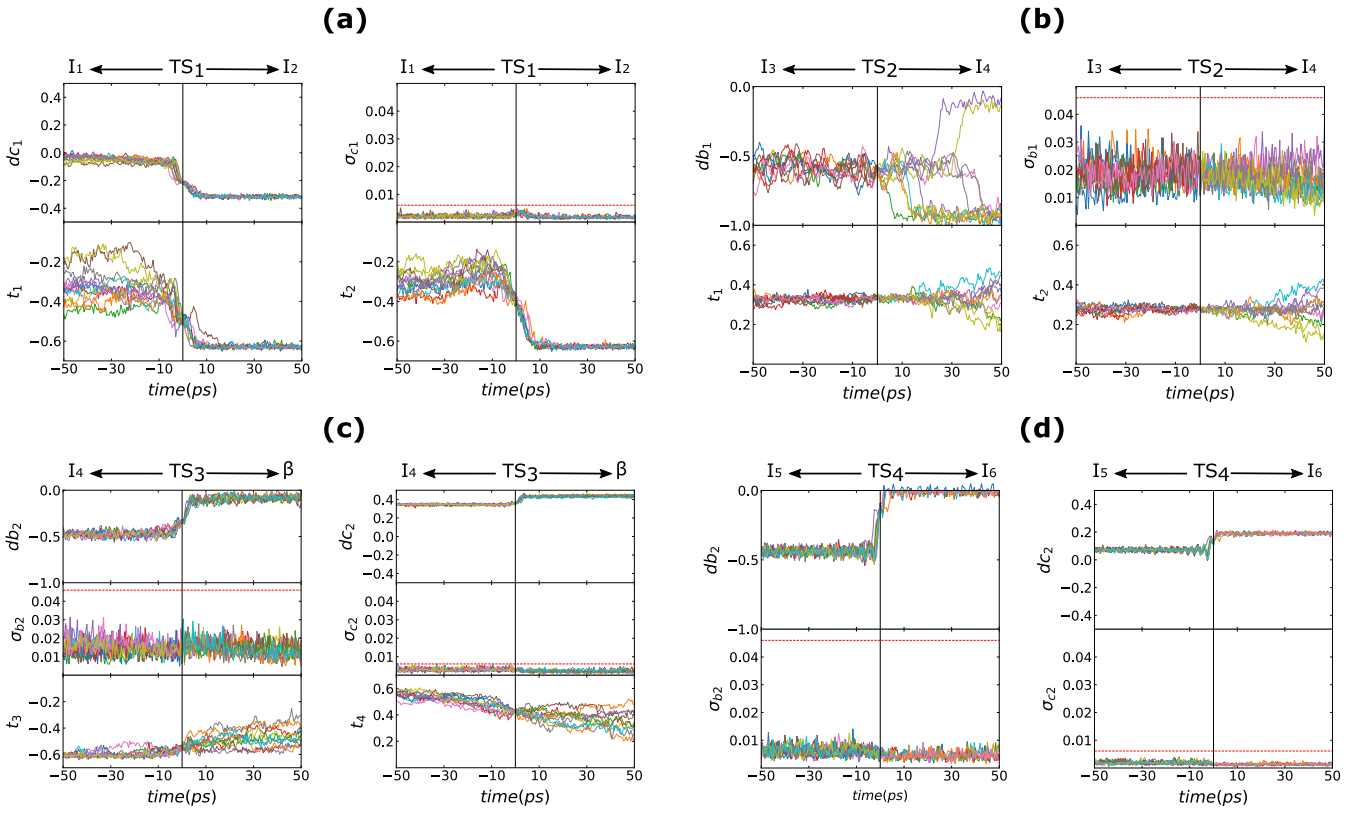

Figure 6. Progress of collective variables and the variance parameters during unbiased simulations starting from (a) TS_1, (b) TS_2, (c) TS_3, and (d) TS_4. The - and + sides of the time axis correspond to transitions from *TS* to the α and β states, respectively. The red dotted lines indicate the highest variance.

respectively, and the index i specifies the interface in which the changes occur. The variance corresponding to the shifts in d_{bi} and d_{ci} is indicated similarly using σ_{bi} and σ_{ci}. Additionally, $t_i = t_{\alpha,i} - t_{\beta,i}$ is a measure for the configurations in each layer, where $t_i = -0.6$ corresponds to all molecules in a β configuration and $t_i = 0.6$ corresponds to all molecules in an α configuration. This way, t_1 and t_2 represent the first interface and t_3 and t_4 correspond to the second one. At $t = 0$, the simulations start in the initial configuration or TS_i. The lines in various colors represent different trajectories that start from the same configuration in the transition state. These trajectories begin with different initial velocities, which are part of the Boltzmann distribution at 250 K. To ensure reliable results, we conducted a total of 20 trajectories for each transition state, aiming to gather adequate statistical data. To distinguish the trajectories that progress toward α from the trajectories toward β, the former are plotted as a negative time propagation while the latter are plotted using the normal positive time propagation. This is purely for visualization purposes and does not reflect the time propagation in the simulations. The red dashed lines indicate the ranges in σ values as discussed in Section 3.

TS_1—Changes in d_c and t. TS_1 connects two minima that mainly change in s (Figure 6a). The transition from $I_1 \rightarrow TS_1 \rightarrow I_2$ is mainly due to a shift along d_c toward β and an increase in the number of molecules in the β conformation. The shift of the first interface results in changes in d_{c1} from 0.0 to −0.32. In other words, this interface has transitioned from the α state to an intermediate state closer to the β. Additionally, this shift appears to enforce minor rotational changes. The transition from TS_1 in both directions is accompanied by a decrease in σ_{c1}. The initial starting point was taken from the umbrella sampling and accidentally had a relatively high variance in d_{c1}. The system quickly recovers, and the sulfur atoms in the layer nicely line up as reflected by the decrease in σ_{c1}. The structures of I_1, TS_1, and I_2 are shown in Figure S1, and these reveal that in the TS_1, the molecules are slightly scattered along c whereas, in I_1 and I_2, they are indeed well aligned. The I_1 structure has a higher rotational disorder which is also evident in the increased values of t_1 and t_2 during $TS_1 \rightarrow I_1$, whereas in the transition toward I_2, all molecules rapidly change to the β configurations. The torsions in the other interface remain unchanged, thereby keeping t_3 and t_4 unaffected. For $TS_1 \rightarrow I_1$, the shifts exhibit faster dynamics than rotations, with changes in dc_1 occurring in 5 ps, whereas the changes in t_1 and t_2 mostly occur in the first 10 ps and on longer time scales. For $TS_1 \rightarrow I_2$, they occur at similar time scales.

TS_2—Changes in d_b. TS_2 separates minima, which are primarily different in d_b (Figure 6b). Figure S2 illustrates a clear shift in $I_3 \rightarrow TS_2 \rightarrow I_4$ within the first interface. Both I_3 and TS_2 show very similar structures with a value of $d_{b1} = -0.5$. The β state is reached when the first interface shifts toward $d_{b1} = 0$ or $d_{b2} = -1$ (Figure 6b). In contrast to the shifts in d_{c1} starting from TS_1, the shift in d_{b1} does not immediately start but occurs at different times due to the relatively flat free energy surface underlying the entire transition. However, once a shift is initiated, it proceeds rapidly on a time scale comparable to that observed in TS_1. The movement of layers parallel to the b axis is much less concerted than that along c. This is reflected by the fluctuations in both σ_{b1} and db_1, especially going toward I_3. The rapid transition toward I_4 and the relatively small values of σ_{b1} throughout the transition suggest that the larger movement might be cooperative. The

https://doi.org/10.1021/acsomega.3c04846
ACS Omega 2024, 9, 3229−3239

torsional changing again occurs in the layers that have shifted, but they occur at different time scales. The gradual increase or decrease in t_1 and t_2 coupled with their larger magnitude of changes with respect to σ_{b1} indicates a molecule-by-molecule mechanism.

TS_3 and TS_4—Changes in d_b, d_c. The trajectories starting from TS_3 and TS_4 confirm the trends found in the previous two examples, but this time changes occur in both planes: changes in d_b, d_c, and torsional changes for TS_3 (Figure S3) and variations of d_b and d_c for TS_4 (Figure S4). According to Figure 6c,d, the changes in d_b and d_c occur rapidly and are likely concerted, whereas the torsional changes are on a much longer time scale and are likely molecule-by-molecule. In all cases, the torsional changes are limited to the interfaces where also shifts occur, and hence they appear to be triggered by these shifts and possibly by torsional changes of neighboring molecules.

The spontaneous shift in d_{b2} does not lead to significant changes in the absolute value of σ_{b2} but is accompanied by a wide fluctuation in this parameter. On the other hand, σ_{c2} fluctuates within a much narrower range. This is probably due to the lower energy barriers for the shift in d_b compared to d_c.

In conclusion, these trajectories show that the shifts along b and c most likely go through a fast cooperative motion, whereas the rotational changes appear to be triggered by movement within the interface, either other rotational changes or shifts with respect to the neighboring interface, but they proceed in a molecule-by-molecule fashion, as can be seen by the much more gradual but significant changes in t_i.

CONCLUSIONS: WHAT IS THE PHASE TRANSITION MECHANISM?

The analysis of the scaling behavior in the transition states, along with committer analysis, has allowed us to understand the thermodynamic, kinetic, and structural characteristics involved in the phase transition. The free energy of the transition states predominantly scales in proportion to the system size, resulting in an almost constant energy barrier per molecule. With this, we arrive at a cooperative mechanism aligned with what experiments suggest in defect-free crystals. Through committer analysis, we can differentiate between a zip-like and cooperative mechanism for the shifts and a molecule-by-molecule or concerted mechanism for the torsional changes. The shifts go likely through a cooperative mechanism, although the fluctuations in db_i and the higher values of σ_{bi} compared to σ_{ci} suggest that the number of molecules to move cooperatively is smaller in the case of a shift along b than along c. This is likely indicative of a lower edge-free energy to break the stacking pattern, and indeed the snapshots of the transition states show a much larger degree of disorder in the aliphatic chains for the (a, b) projections than for the (a, c) projections. The classical nucleation-and-growth picture can be married with the cooperative mechanism by introducing the concept of the "critical cooperative segment".[47] This is a group of molecules that move cooperatively, after which the rest of the crystal can transform. The size of the segment is highly dependent on the edge-free energy to create such a segment, which in turn depends on the energetics involved and the defect density.[67]

For the defect-free systems, the critical cooperative segment for transitions in d_c is much larger than that for d_b. The nonlinear scaling of the $I_3 \rightarrow TS_2$ in Table 2 is an indication of this, where a length of 4 replications in b is smaller than the critical cooperative segment and a length of 8 replications is larger.

The torsional changes appear to proceed in a kind of cascading mechanism, where the movement of one torsion or movement in an interface triggers further conversion. Additionally, the transition rate for shifts is twice as fast as the rate of rotations.

It should be noted that in the study conducted by Shi et al., they distinguish between the cooperative and the nucleation-and-growth mechanisms with respect to the defect density of the crystal. The former occurs in the vdW connections, and the latter occurs in the hydrogen-bonding pattern. The entire focus of our work has been on a defect-free crystal. Consequently, the phase transition affects the vdW connections, while the hydrogen-bonded middles stay intact. From a thermodynamic standpoint, the scaling of the free energy barriers, which we obtained, and the DSC measurements conducted by Shi's group suggest a cooperative mechanism for a defect-free crystal. However, by resolving the phase transition into fundamental transformations within the vdW intervals, we successfully determined the relative cooperativity and molecule-by-molecule characteristics of shifts and rotations. Again in both studies, shifts are found to be cooperative, while the rotations in a defect-free crystal, as observed in our study, and the alteration of the hydrogen bonds in crystals with high defect density, observed in Shi's study, both follow a nucleation-and-growth mechanism. In our previous study, we provided more experimental proof by reproducing the IR and Raman spectra of the stable states.[69] Also, the energy barriers coming from Shi's measurements and our calculations are also comparable as discussed above. It is not easy to gather more experimental evidence, since what we inspect occurs at an atomic scale.

In the end, we believe that the behavior observed in DL-methionine is likely applicable to phase transitions in other layered systems, which interact through aliphatic chains as well.

ASSOCIATED CONTENT

Supporting Information

The Supporting Information is available free of charge at https://pubs.acs.org/doi/10.1021/acsomega.3c04846.

> The structural differences in the $I_1 \rightarrow TS_1 \rightarrow I_2$ transition in the $a-c$ projection (Figure S1); $I_3 \rightarrow TS_2 \rightarrow I_4$ transition in the $a-b$ projection (Figure S2); $I_4 \rightarrow TS_3 \rightarrow \beta$ transition in the $a-b$ and $a-c$ projection (Figure S3); $I_5 \rightarrow TS_4 \rightarrow I_6$ transition in the $a-b$ and $a-c$ projections (Figure S4); Harmonic force constants used for each CVs and in each system (Table S1) (PDF)

AUTHOR INFORMATION

Corresponding Author

Herma M. Cuppen − *Faculty of Science, Institute for Molecules and Materials, Radboud University, Nijmegen 6500 HC, The Netherlands; Computational Chemistry Group, Van't Hoff Institute for Molecular Sciences, University of Amsterdam, Amsterdam 1090 GD, The Netherlands;* orcid.org/0000-0003-4397-0739; Phone: +31 024-3653035; Email: h.cuppen@science.ru.nl

https://doi.org/10.1021/acsomega.3c04846
ACS Omega 2024, 9, 3229−3239

Author

Saba Ghasemlou − *Faculty of Science, Institute for Molecules and Materials, Radboud University, Nijmegen 6500 HC, The Netherlands;* orcid.org/0000-0002-6184-2549

Complete contact information is available at: https://pubs.acs.org/10.1021/acsomega.3c04846

Notes

The authors declare no competing financial interest.

■ ACKNOWLEDGMENTS

This research was funded by Institute for Molecules and Materials (IMM), Radboud University. The authors thank Bernd Ensing and Alberto Pérez de Alba Ortz from the University of Amsterdam for the useful discussions and feedback.

■ REFERENCES

(1) Vippagunta, S. R.; Brittain, H. G.; Grant, D. J. Crystalline solids. *Adv. Drug Delivery Rev.* **2001**, *48*, 3−26.

(2) Cruz-Cabeza, A. J.; Bernstein, J. Conformational polymorphism. *Chem. Rev.* **2014**, *114*, 2170−2191.

(3) Wang, H.; Pan, Q.; Wu, Q.; Zhang, X.; Huang, Y.; Lushington, A.; Li, Q.; Sun, X. Ultrasmall MoS2 embedded in carbon nanosheets-coated Sn/SnOx as anode material for high-rate and long life Li-ion batteries. *J. Mater. Chem. A* **2017**, *5*, 4576−4582.

(4) Bučar, D.; Lancaster, R. W.; Bernstein, J. Disappearing polymorphs revisited. *Angew. Chem., Int. Ed.* **2015**, *54*, 6972−6993.

(5) Bauer, J.; Spanton, S.; Henry, R.; Quick, J.; Dziki, W.; Porter, W.; Morris, J. Ritonavir: an extraordinary example of conformational polymorphism. *Pharm. Res.* **2001**, *18*, 859−866.

(6) Dunitz, J. D.; Bernstein, J. Disappearing polymorphs. *Acc. Chem. Res.* **1995**, *28*, 193−200.

(7) Bernstein, J. *Polymorphism in Molecular Crystals*; Oxford University Press, 2007.

(8) Luong, L. M.; Olmstead, M. M.; Balch, A. L. A non-luminescent polymorph of [(cyclohexyl isocyanide) 2 Au] PF 6 that becomes luminescent upon grinding or exposure to dichloromethane vapor. *Chem. Commun.* **2020**, *57*, 793−796.

(9) Hondoh, H.; Ueno, S. Polymorphism of edible fat crystals. *Progress in Crystal Growth and Characterization of Materials* **2016**, *62*, 398−399. Special Issue: Recent Progress on Fundamentals and Applications of Crystal Growth; Proceedings of the 16th International Summer School on Crystal Growth (ISSCG-16).

(10) Ehrenfest, P. Phase changes in the ordinary and extended sense classified according to the corresponding singularities of the thermodynamic potential. *Proc. Acad. Sci. Amsterdam* **1933**, 153−157.

(11) Mnyukh, Y. *Fundamentals of Solid-state Phase Transitions, Ferromagnetism and Ferroelectricity*; Authorhouse, 2001.

(12) Mnyukh, Y. Mechanism and kinetics of phase transitions and other reactions in solids. 2011, arXiv:1110.1654. arXiv.org e-Print archive. https://arxiv.org/abs/1110.1654.

(13) Anwar, J.; Tuble, S. C.; Kendrick, J. Concerted molecular displacements in a thermally-induced solid-state transformation in crystals of DL-norleucine. *J. Am. Chem. Soc.* **2007**, *129*, 2542−2547.

(14) Zahn, D.; Anwar, J. Collective displacements in a molecular crystal polymorphic transformation. *RSC Adv.* **2013**, *3*, 12810−12815.

(15) Paukov, I. E.; Kovalevskaya, Y. A.; Drebushchak, V. A.; Drebushchak, T. N.; Boldyreva, E. V. An extended phase transition in crystalline L-cysteine near 70 K. *J. Phys. Chem. B* **2007**, *111*, 9186−9188.

(16) Kolesov, B. A.; Minkov, V. S.; Boldyreva, E. V.; Drebushchak, T. N. Phase transitions in the crystals of L-and DL-cysteine on cooling: intermolecular hydrogen bonds distortions and the side-chain motions of thiol-groups. 1. L-cysteine. *J. Phys. Chem. B* **2008**, *112*, 12827−12839.

(17) Dunitz, J. D. Phase transitions in molecular crystals from a chemical viewpoint. *Pure Appl. Chem.* **1991**, *63*, 177−185.

(18) Görbitz, C. H. Solid-state phase transitions in DL-norvaline studied by single-crystal X-ray diffraction. *J. Phys. Chem. B* **2011**, *115*, 2447−2453.

(19) Drebushchak, T. N.; Pankrushina, N.; Boldyreva, E. A new type of polymorphic transformation in tolbutamide: Unusual low-temperature conformation ordering. *Doklady Phys. Chem.* **2011**, *437*, 61−64.

(20) Drebushchak, T. N.; Drebushchak, V. A.; Boldyreva, E. V. Solid-state transformations in the *β*-form of chlorpropamide on cooling to 100 K. *Acta Crystallogr. Sect. B: Struct. Sci.* **2011**, *67*, 163−176.

(21) Zakharov, B. A.; Losev, E. A.; Kolesov, B. A.; Drebushchak, V. A.; Boldyreva, E. V. Low-temperature phase transition in glycine—glutaric acid co-crystals studied by single-crystal X-ray diffraction, Raman spectroscopy and differential scanning calorimetry. *Acta Crystallogr. Sect. B: Struct. Sci.* **2012**, *68*, 287−296.

(22) Barthes, M.; Bordallo, H.; Dénoyer, F.; Lorenzo, J.-E.; Zaccaro, J.; Robert, A.; Zontone, F. Micro-transitions or breathers in L-alanine? *Eur. Phys. J. B* **2003**, *37*, 375−382.

(23) Chatzigeorgiou, P.; Papakonstantopoulos, N.; Tagaroulia, N.; Pollatos, E.; Xynogalas, P.; Viras, K. Solid- solid phase transitions in dl-norvaline studied by differential scanning calorimetry and Raman spectroscopy. *J. Phys. Chem. B* **2010**, *114*, 1294−1300.

(24) Coles, S. J.; Gelbrich, T.; Griesser, U.; Hursthouse, M.; Pitak, M.; Threlfall, T. The elusive high temperature solid-state structure of D, L-Norleucine. *Cryst. Growth Des.* **2009**, *9*, 4610−4612.

(25) Chopra, D.; Row, T. G. Disorder induced concomitant polymorphism in 3-fluoro-N-(3-fluorophenyl) benzamide. *Cryst. Growth Des.* **2008**, *8*, 848−853.

(26) Das, D.; Jacobs, T.; Pietraszko, A.; Barbour, L. J. Anomalous thermal expansion of an organic crystal-implications for elucidating the mechanism of an enantiotropic phase transformation. *Chem. Commun.* **2011**, *47*, 6009−6011.

(27) Caira, M. R.; Bettinetti, G.; Sorrenti, M.; Catenacci, L. Order-disorder enantiotropy, monotropy, and isostructurality in a tetroxoprim-sulfametrole 1:1 molecular complex: Crystallographic and thermal studies. *J. Pharm. Sci.* **2003**, *92*, 2164−2176.

(28) Gardon, M.; Pinheiro, C. B.; Chapuis, G. Structural phases of hexamethylenetetramine-pimelic acid (1/1): a unified description based on a stacking model. *Acta Crystallogr. Sect. B: Struct. Sci.* **2003**, *59*, 527−536.

(29) Vrcelj, R. M.; Clark, N. I.; Kennedy, A. R.; Sheen, D. B.; Shepherd, E. E.; Sherwood, J. N. Two New Paracetamol/Dioxane Solvates—a System Exhibiting a Reversible Solid-State Phase Transformation. *J. Pharm. Sci.* **2003**, *92*, 2069−2073.

(30) Martins, D.; Sanselme, M.; Houssin, O.; Dupray, V.; Petit, M.; Pasquier, D.; Diolez, C.; Coquerel, G. Physical transformations of the active pharmaceutical ingredient BN83495: enantiotropic and monotropic relationships. Access to several polymorphic forms by using various solvation−desolvation processes. *CrystEngComm* **2012**, *14*, 2507−2519.

(31) Rubin-Preminger, J. M.; Bernstein, J.; Harris, R. K.; Evans, I. R.; Ghi, P. Y. [R, S]-ethambutol dihydrochloride: Variable-temperature studies of a dimorphic system with very similar packing. *J. Pharm. Sci.* **2004**, *93*, 2810−2819.

(32) Katrusiak, A. Conformational transformation coupled with the order-disorder phase transition in 2-methyl-1, 3-cyclohexanedione crystals. *Acta Crystallogr. Sect. B: Struct. Sci.* **2000**, *56*, 872−881.

(33) Schmidt, A.; Kababya, S.; Appel, M.; Khatib, S.; Botoshansky, M.; Eichen, Y. Measuring the temperature width of a first-order single crystal to single crystal phase transition using solid-state NMR: Application to the polymorphism of 2-(2, 4-dinitrobenzyl)-3-methylpyridine. *J. Am. Chem. Soc.* **1999**, *121*, 11291−11299.

(34) Srinivasa Gopalan, R.; Kumaradhas, P.; Kulkarni, G. Structural phase transition in adipic acid. *J. Solid State Chem.* **1999**, *148*, 129−134.

(35) Takahashi, H.; Ito, Y. Low-temperature-induced reversible single-crystal-to-single-crystal phase transition of 3, 4-dichloro-2; 4; 6-triethylbenzophenone. *CrystEngComm* **2010**, *12*, 1628−1634.
(36) Kaftory, M.; Botoshansky, M.; Kapon, M.; Shteiman, V. Irreversible single-crystal to polycrystal and reversible single-crystal to single-crystal phase transformations in cyanurates. *Acta Crystallogr. Sect. B: Struct. Sci.* **2001**, *57*, 791−799.
(37) Steiner, T.; Hinrichs, W.; Saenger, W.; Gigg, R. Jumping crystals': X-ray structures of the three crystalline phases of (±)-3, 4-di-O-acetyl-1, 2, 5, 6-tetra-O-benzyl-myo-inositol. *Acta Crystallogr. Sect. B: Struct. Sci.* **1993**, *49*, 708−718.
(38) Skoko, Ž.; Zamir, S.; Naumov, P.; Bernstein, J. The thermosalient phenomenon."Jumping crystals" and crystal chemistry of the anticholinergic agent oxitropium bromide. *J. Am. Chem. Soc.* **2010**, *132*, 14191−14202.
(39) Halasz, I. Single-crystal-to-single-crystal reactivity: gray, rather than black or white. *Cryst. Growth Des.* **2010**, *10*, 2817−2823.
(40) Takahashi, H.; Tamura, R.; Yabunaka, S.; Ushio, T. Crystal structure of a new racemate showing Preferential Enrichment: evidence for the existence as a racemic mixed crystal composed of the two enantiomers. *Mendeleev Commun.* **2003**, *13*, 119−121.
(41) Enjalbert, R.; Galy, J. CH3CN: X-ray structural investigation of a unique single crystal. $\beta \rightarrow \alpha$ phase transition and crystal structure. *Acta Crystallogr. Sect. B: Struct. Sci.* **2002**, *58*, 1005−1010.
(42) Hashizume, D.; Miki, N.; Yamazaki, T.; Aoyagi, Y.; Arisato, T.; Uchiyama, H.; Endo, T.; Yasui, M.; Iwasaki, F. Mechanism of the first-order phase transition of an acylurea derivative: observation of intermediate stages of transformation with a detailed temperature-resolved single-crystal diffraction method. *Acta Crystallogr. Sect. B: Struct. Sci.* **2003**, *59*, 404−415.
(43) Fernandes, M. A.; Levendis, D. C.; Schoening, F. L. A new polymorph of ortho-ethoxy-trans-cinnamic acid: single-to-single-crystal phase transformation and mechanism. *Acta Crystallogr. Sect. B: Struct. Sci.* **2004**, *60*, 300−314.
(44) Garcia-Garibay, M. A. Molecular crystals on the move: from single-crystal-to-single-crystal photoreactions to molecular machinery. *Angew. Chem., Int. Ed.* **2007**, *46*, 8945−8947.
(45) van den Ende, J. A.; Smets, M. M.; de Jong, D. T.; Brugman, S. J.; Ensing, B.; Tinnemans, P. T.; Meekes, H.; Cuppen, H. M. Do solid-to-solid polymorphic transitions in DL-norleucine proceed through nucleation? *Faraday Discuss.* **2015**, *179*, 421−436.
(46) Cuppen, H. M.; Smets, M. M.; Krieger, A. M.; van den Ende, J. A.; Meekes, H.; van Eck, E. R.; Görbitz, C. H. The rich solid-state phase behavior of l-phenylalanine: disappearing polymorphs and high temperature forms. *Cryst. Growth Des.* **2019**, *19*, 1709−1719.
(47) Smets, M. M. H.; Kalkman, E.; Krieger, A.; Tinnemans, P.; Meekes, H.; Vlieg, E.; Cuppen, H. On the mechanism of solid-state phase transitions in molecular crystals-the role of cooperative motion in (quasi) racemic linear amino acids. *IUCrJ.* **2020**, *7*, 331−341, DOI: 10.1107/S2052252520001335.
(48) Brandel, C.; Cartigny, Y.; Couvrat, N.; Eusebio, M. E. S.; Canotilho, J.; Petit, S.; Coquerel, G. Mechanisms of reversible phase transitions in molecular crystals: case of ciclopirox. *Chem. Mater.* **2015**, *27*, 6360−6373.
(49) Sato, O. Dynamic molecular crystals with switchable physical properties. *Nat. Chem.* **2016**, *8*, 644−656.
(50) Lakshmipathi, M.; Sk, A. I.; Kundu, P. K.; Tothadi, S.; Ghosh, S. Mechanically Elastic and Light-Induced Bending of Acylhydrazone-Based Photoswitch Crystal. *Cryst. Growth Des.* **2023**, *23*, 4939−4945, DOI: 10.1021/acs.cgd.3c00196.
(51) Takazawa, K.; Inoue, J.-i.; Mitsuishi, K.; Yoshida, Y.; Kishida, H.; Tinnemans, P.; Engelkamp, H.; Christianen, P. C. Phase-transition-induced jumping, bending, and wriggling of single crystal nanofibers of coronene. *Sci. Rep.* **2021**, *11*, No. 3175.
(52) Sahoo, S. C.; Sinha, S. B.; Kiran, M.; Ramamurty, U.; Dericioglu, A. F.; Reddy, C. M.; Naumov, P. Kinematic and mechanical profile of the self-actuation of thermosalient crystal twins of 1, 2, 4, 5-tetrabromobenzene: A molecular crystalline analogue of a bimetallic strip. *J. Am. Chem. Soc.* **2013**, *135*, 13843−13850.
(53) Panda, M. K.; Runčevski, T.; Chandra Sahoo, S.; Belik, A. A.; Nath, N. K.; Dinnebier, R. E.; Naumov, P. Colossal positive and negative thermal expansion and thermosalient effect in a pentamorphic organometallic martensite. *Nat. Commun.* **2014**, *5*, No. 4811.
(54) Lan, L.; Li, L.; Di, Q.; Yang, X.; Liu, X.; Naumov, P.; Zhang, H. Organic Single-Crystal Actuators and Waveguides that Operate at Low Temperatures. *Adv. Mater.* **2022**, *34*, No. 2200471.
(55) Karothu, D. P.; Weston, J.; Desta, I. T.; Naumov, P. Shape-memory and self-healing effects in mechanosalient molecular crystals. *J. Am. Chem. Soc.* **2016**, *138*, 13298−13306.
(56) Di, Q.; Li, L.; Miao, X.; Lan, L.; Yu, X.; Liu, B.; Yi, Y.; Naumov, P.; Zhang, H. Fluorescence-based thermal sensing with elastic organic crystals. *Nat. Commun.* **2022**, *13*, No. 5280.
(57) Lan, L.; Yang, X.; Tang, B.; Yu, X.; Liu, X.; Li, L.; Naumov, P.; Zhang, H. Hybrid elastic organic crystals that respond to aerial humidity. *Angew. Chem., Int. Ed.* **2022**, *61*, No. e202200196.
(58) Yang, X.; Lan, L.; Li, L.; Liu, X.; Naumov, P.; Zhang, H. Remote and precise control over morphology and motion of organic crystals by using magnetic field. *Nat. Commun.* **2022**, *13*, No. 2322.
(59) Costil, R.; Holzheimer, M.; Crespi, S.; Simeth, N. A.; Feringa, B. L. Directing coupled motion with light: a key step toward machine-like function. *Chem. Rev.* **2021**, *121*, 13213−13237.
(60) Tong, F.; Kitagawa, D.; Bushnak, I.; Al-Kaysi, R. O.; Bardeen, C. J. Light-Powered Autonomous Flagella-Like Motion of Molecular Crystal Microwires. *Angew. Chem., Int. Ed.* **2021**, *60*, 2414−2423.
(61) Ghosh, S.; Mishra, M. K. Elastic molecular crystals: From serendipity to design to applications. *Cryst. Growth Des.* **2021**, *21*, 2566−2580.
(62) Görbitz, C. H.; Alebachew, F.; Petříček, V. Solid-state phase transitions of DL-aminobutyric acid. *J. Phys. Chem. B* **2012**, *116*, 10715−10721.
(63) Ren, P.; Reichert, D.; He, Q.; Zhang, L.; Tang, H. Understanding the molecular dynamics associated with polymorphic transitions of DL-Norvaline with solid-state NMR methods. *J. Phys. Chem. B* **2011**, *115*, 2814−2823.
(64) Smets, M. M. H.; Brugman, S.; Van Eck, E.; Van Den Ende, J.; Meekes, H.; Cuppen, H. Understanding the Solid-State Phase Transitions of DL-Norleucine: An in Situ DSC, Microscopy, and Solid-State NMR Study. *Cryst. Growth Des.* **2015**, *15*, 5157−5167.
(65) Görbitz, C. H.; Paulsen, J. C.; Borgersen, J. Redetermined crystal structure of β-dl-methionine at 320 K. *Acta Crystallogr., Sect. E: Crystallogr. Commun.* **2015**, *71*, o398−o399.
(66) Lima, R. A.; Vasconcelos, D. L.; da Silva, J. A. S.; Santana, J. V.; Cordeiro, A. J. P.; Ayala, A. P.; Freire, P. T. Crystal structure, vibrational and chemical properties and phase transitions in Glycyl-DL-Aspartic acid and Glycyl-DL-Aspartic acid monohydrated. *J. Mol. Struct.* **2023**, *1286*, No. 135651.
(67) Shi, G.; Li, S.; Shi, P.; Gong, J.; Zhang, M.; Tang, W. Distinct pathways of solid-to-solid phase transitions induced by defects: the case of DL-methionine. *IUCrJ.* **2021**, *8*, 584−594.
(68) Minkov, V. S.; Tumanov, N. A.; Kolesov, B. A.; Boldyreva, E. V.; Bizyaev, S. N. Phase transitions in the crystals of l-and dl-cysteine on cooling: the role of the hydrogen-bond distortions and the side-chain motions. 2. DL-cysteine. *J. Phys. Chem. B* **2009**, *113*, 5262−5272.
(69) Ghasemlou, S.; Ensing, B.; Cuppen, H. Simulation of solid-state phase transition in DL-methionine. *CrystEngComm* **2023**, *25*, 3618−3627, DOI: 10.1039/D3CE00227F.
(70) https://lammps.sandia.gov/cite.html.
(71) Bonomi, M.; Branduardi, D.; Bussi, G.; Camilloni, C.; Provasi, D.; Raiteri, P.; Donadio, D.; Marinelli, F.; Pietrucci, F.; Broglia, R. A.; Parrinello, M. PLUMED: A portable plugin for free-energy calculations with molecular dynamics. *Comput. Phys. Commun.* **2009**, *180*, 1961−1972.
(72) Bonomi, M.; Bussi, G.; Camilloni, C.; Tribello, G. A.; Banáš, P.; Barducci, A.; Bernetti, M.; Bolhuis, P. G.; Bottaro, S.; Branduardi, D.;

et al. Promoting transparency and reproducibility in enhanced molecular simulations. *Nat. Methods* **2019**, *16*, 670−673.
(73) Tribello, G. A.; Bonomi, M.; Branduardi, D.; Camilloni, C.; Bussi, G. PLUMED 2: New feathers for an old bird. *Comput. Phys. Commun.* **2014**, *185*, 604−613.
(74) Humphrey, W.; Dalke, A.; Schulten, K. VMD − Visual Molecular Dynamics. *J. Mol. Graphics* **1996**, *14*, 33−38.
(75) Stone, J. An Efficient Library for Parallel Ray Tracing and Animation; M.Sc. thesis, Computer Science Department, University of Missouri-Rolla, 1998.
(76) Stone, J.; Gullingsrud, J.; Grayson, P.; Schulten, K. *A System for Interactive Molecular Dynamics Simulation*, 2001 ACM Symposium on Interactive 3D Graphics. New York, 2001; 191−194.
(77) Eargle, J.; Wright, D.; Luthey-Schulten, Z. Multiple Alignment of protein structures and sequences for VMD. *Bioinformatics* **2006**, *22*, 504−506.
(78) Frishman, D.; Argos, P. Knowledge-based secondary structure assignment. *Proteins: Struct., Funct., Genet.* **1995**, *23*, 566−579.
(79) Varshney, A.; Brooks, F. P.; Wright, W. V. Linearly Scalable Computation of Smooth Molecular Surfaces. *IEEE Comput. Graph. Appl.* **1994**, *14*, 19−25.
(80) Sanner, M. F.; Olsen, A.; Spehner, J.-C.In *Fast and Robust Computation of Molecular Surfaces*, Proceedings of the 11th ACM Symposium on Computational Geometry. New York, 1995; pp C6−C7.
(81) Sharma, R.; Zeller, M.; Pavlovic, V. I.; Huang, T. S.; Lo, Z.; Chu, S.; Zhao, Y.; Phillips, J. C.; Schulten, K. Speech/Gesture Interface to a Visual-Computing Environment. *IEEE Comput. Grap. Appl.* **2000**, *20*, 29−37.
(82) Wang, J.; Wolf, R. M.; Caldwell, J. W.; Kollman, P. A.; Case, D. A. Development and testing of a general amber force field. *J. Comput. Chem.* **2004**, *25*, 1157−1174.
(83) Bayly, C. I.; Cieplak, P.; Cornell, W.; Kollman, P. A. A well-behaved electrostatic potential based method using charge restraints for deriving atomic charges: the RESP model. *J. Phys. Chem. A* **1993**, *97*, 10269−10280.
(84) Gilson, M. K.; Gilson, H. S.; Potter, M. J. Fast assignment of accurate partial atomic charges: an electronegativity equalization method that accounts for alternate resonance forms. *J. Chem. Inf. Comput. Sci.* **2003**, *43*, 1982−1997.
(85) Debiec, K. T.; Cerutti, D. S.; Baker, L. R.; Gronenborn, A. M.; Case, D. A.; Chong, L. T. Further along the road less traveled: AMBER ff15ipq, an original protein force field built on a self-consistent physical model. *J. Chem. Theory Comput.* **2016**, *12*, 3926−3947.
(86) in't Veld, P. J.; Ismail, A. E.; Grest, G. S. Application of Ewald summations to long-range dispersion forces. *J. Chem. Phys.* **2007**, *127*, No. 144711, DOI: 10.1063/1.2770730.
(87) Posch, H. A.; Hoover, W. G.; Vesely, F. J. Canonical dynamics of the Nosé oscillator: Stability, order, and chaos. *Phys. Rev. A* **1986**, *33*, 4253.
(88) Roux, B. The calculation of the potential of mean force using computer simulations. *Comput. Phys. Commun.* **1995**, *91*, 275−282.
(89) Smets, M. M. H.; Brugman, S.; Van Eck, E.; Tinnemans, P.; Meekes, H.; Cuppen, H. Understanding the single-crystal-to-single-crystal solid-state phase transition of DL-methionine. *CrystEngComm* **2016**, *18*, 9363−9373.
(90) Görbitz, C. H.; Qi, L.; Mai, N. T. K.; Kristiansen, H. Redetermined crystal structure of α-DL-methionine at 340 K. *Acta Crystallogr., Sect. E: Struct. Rep. Online* **2014**, *70*, 337−340.

https://doi.org/10.1021/acsomega.3c04846
ACS Omega 2024, 9, 3229−3239